

## Formation of multiple BGK-like structures in the time-asymptotic state of collisionless Vlasov-Poisson plasmas

Hugo A. Carril <sup>\*</sup>, Jorge A. Gidi <sup>†</sup>, Roberto E. Navarro <sup>‡</sup>, and Jaime A. Araneda <sup>§</sup>

*Departamento de Física, Facultad de Ciencias Físicas y Matemáticas, Universidad de Concepción, Concepción 4070386, Chile*



(Received 25 April 2023; accepted 10 May 2023; published 7 June 2023)

The time-asymptotic state of a finite-amplitude perturbation in a collisionless and Maxwellian plasma is typically represented as a steady state of two nonlinearly superposed, counterpropagating Bernstein-Greene-Kruskal (BGK) modes. Using high-resolution Vlasov-Poisson simulations, we show that the plasma evolves self-consistently into a time-asymptotic state of multiple vortexlike structures that gradually fill the phase space and reduce filamentation. This occurs without the need for external forcing or the presence of an energetic plasma population. This finding suggests that the time-asymptotic regime of the plasma is rather akin to a nonlinear superposition of multiple BGK-like modes associated with nearly constant phase-speed waves. The electric field and the space-averaged particle distribution function exhibit a power-law broad spectrum, which is consistent with an energy cascade towards smaller scales in both position and velocity spaces.

DOI: [10.1103/PhysRevE.107.065203](https://doi.org/10.1103/PhysRevE.107.065203)

### I. INTRODUCTION

Finite-amplitude spatial perturbations or external forcing in a collisionless plasma can lead to undamped, solitary, and nonlinear states in which resonant particles become trapped in potential wells. This is observed as localized vortices or holes in the phase space of particles, which can last for long periods of time [1–5]. In particular, this situation is found during the nonlinear Landau damping of Langmuir waves, in which an initial electrostatic perturbation on an unmagnetized electron plasma leads to a saturated state where electrons are trapped by the electrostatic potential around the phase speed of the perturbed wave mode [1,6–8]. Similar phenomena have been found in observational research as trapping of electrons along the magnetic field lines in near-Earth environments [9–15], in experimental research dedicated to Landau damping and particle trapping [16–18], in electron beam injection into low- $\beta$  plasma columns [19], and in simulations of collisionless electron plasmas with Maxwellian [1,20–22] and non-Maxwellian distribution functions [3,4,23,24].

Phase-space vortices in electrostatic plasmas are exact solutions of the one-dimensional Vlasov-Poisson system of equations known as Bernstein-Greene-Kruskal (BGK) states [25–28]. For a BGK state to be stable the distribution function of the trapped particles must not be monotonically decreasing [29], and the background distribution supporting particle trapping must have less than three maxima [30]. These conditions allow the propagation of stable phase-space holes for long times in plasmas with single-maximum distributions, such as Maxwellian distributions [30].

The long-time stability of one-dimensional BGKs are affected by numerical diffusive effects caused by the finite resolution of the position and velocity grids, modifying the phase-space structures observed in Vlasov-Poisson simulations [31–33]. Also, multiple one-dimensional phase-space holes are unstable to the growth of sidebands, which disrupt the state by merging the holes when the wavelength of the perturbations is smaller than the length of the spatial domain [34–36]. Indeed, it has been observed that multiple neighboring BGK structures evolve toward a time-asymptotic state consisting of a single stable hole in long-term Vlasov-Poisson simulations [37].

The formation of multiple regions of particle trapping in the distribution function can be approximately represented as a nonlinear superposition of individual BGK modes, where the electrostatic potentials are linearly superposed and the distribution function is built in a piecewise way [38,39]. This approximation is supported by Vlasov simulations [35,40–42] and by theoretical works [2,7,43,44]. However, this nonlinear superposition does not capture all structures formed in the distribution function [40,41].

This work addresses a long-standing academic question about the long-time evolution of the nonlinear Landau damping problem. To date, there are two known paradigms describing the time-asymptotic state of one-dimensional Maxwellian electron plasmas undergoing nonlinear Landau damping. One of them states that the time-asymptotic state corresponds to a nonlinear superposition of two individual counterpropagating BGK states [1]. In this case, the phase space develops stable vortical structures after Landau damping stops [20], with the space-averaged distributions exhibiting characteristic plateaus at velocities around the BGK's phase velocities [1,3,32,35]. The second paradigm states that the time-asymptotic state is akin to a nonlinear superposition of multiple BGK states [2,43].

Our results suggest that the physical picture of the time-asymptotic state of collisionless Vlasov-Poisson plasmas is far

\*hcarril@udec.cl

†jorgegidi@udec.cl

‡roberto.navarro@udec.cl

§jaraneda@udec.cl

richer than the standard view of two stable BGK modes only, thus rather akin to the framework of multiple BGK-like states [2]. Indeed, it is shown that multiple small phase-space holes occur in a wide range of velocities below the Langmuir phase speed,  $|v| < v_L$ . Each hole is associated with electron plasma waves (EPWs) whose phase speeds are similar to the propagation speed of the corresponding holes. The electric field reaches a time-asymptotic state characterized by a power-law energy spectrum, indicating an energy cascade process. In addition, the space-averaged distribution function exhibits a piecewise power-law velocity spectrum, showing a reduction in phase-space filamentation, suggesting that the development of small-scale electron holes is self-similar and intermittent.

## II. VLASOV-POISSON NUMERICAL SIMULATIONS

The propagation of high-frequency oscillations in collisionless and unmagnetized plasmas is studied in terms of the one-dimensional Vlasov-Poisson system of equations:

$$\frac{\partial f}{\partial t} + v \frac{\partial f}{\partial x} + \frac{e}{m} \frac{\partial \phi}{\partial x} \frac{\partial f}{\partial v} = 0, \quad (1)$$

$$\frac{\partial^2 \phi}{\partial x^2} = 4\pi e \left( \int_{-\infty}^{\infty} dv f - n_0 \right), \quad (2)$$

where  $f = f(x, v, t)$  is the electron phase-space distribution function;  $\phi = \phi(x, t)$  is the electrostatic potential; and  $-e$ ,  $m$ , and  $n_0$  are the charge, mass, and density of electrons, respectively. The ions are considered as a motionless neutralizing background with density  $n_i = n_0$ , and periodic boundary conditions are assumed in  $x$ .

To solve Eqs. (1) and (2), an FFT pseudospectral code was written in the Julia programming language [45]. A semi-Lagrangian splitting scheme is employed [46], with spectral interpolation in the Fourier transformed phase space. The time advance is performed using an optimized second-order symplectic integrator [47]. Spectral interpolation introduces an exponential error that decreases with the number of nodes [48,49], so that less error is achieved for the same number of nodes compared to, for example, polynomial-spline interpolation. A Gaussian-like filter of the form  $e^{-36(v/v_{\max})^{36}}$  [50] is used to smooth out abrupt variations of the velocity distribution function at small velocity scales, where  $v$  is the conjugate variable of  $x$  and  $v_{\max}$  is the maximum allowed value of  $v$ . Although not shown here, the Vlasov code has been successfully tested on several problems, e.g., Manfredi [1], Raghunathan and Ganesh [3], Galeotti and Califano [32], Rupp *et al.* [20], Califano *et al.* [33], among others.

The initially single-mode perturbed electron phase-space distribution is

$$f(x, v, 0) = f_0(v)[1 + \varepsilon \cos(k_1 x)], \quad (3)$$

where  $\varepsilon$  and  $k_1$  are the amplitude and wave number of the perturbation, respectively, and  $f_0(v)$  the unperturbed Maxwellian distribution function,

$$f_0(v) = \frac{n_0}{\sqrt{2\pi} v_{\text{th}}} \exp\left(-\frac{v^2}{2v_{\text{th}}^2}\right), \quad (4)$$

where  $v_{\text{th}} = \sqrt{k_B T/m}$  is the electron thermal speed,  $k_B$  the Boltzmann constant, and  $T$  the electron temperature.

Simulations are performed with a box-length  $L = 2\pi/k_1$ , and velocity domain  $|v|/v_{\text{th}} < 7.7$ ; phase space is discretized into  $N_x = 2^{11} = 2048$  and  $N_v = 2^{17} = 131\,072$  grid points in the space and velocity components, respectively; the time step is  $\omega_p \Delta t = 0.05$ , with a maximum time simulation run of  $\omega_p t_{\max} = 14\,000$ , where  $\omega_p = \sqrt{4\pi e^2 n_0/m}$  is the electron plasma frequency; and perturbation parameters are  $\varepsilon = 0.04$  and  $k_1 v_{\text{th}}/\omega_p = 0.4$ . The effects of changing the velocity grid resolution  $2^{11} \leq N_v \leq 2^{17}$  on the formation of phase-space holes are shown in later sections.

## III. NONLINEAR LANDAU DAMPING

Figure 1(a) shows the time evolution of the first Fourier mode of the electrostatic potential in a long-time simulation. Initially, two counterpropagating Langmuir waves are excited with frequencies  $\omega_L/\omega_p \simeq \pm 1.285$  and phase speeds  $|v_L/v_{\text{th}}| \simeq 3.213$ . The energy decreases monotonously with damping rate  $\gamma_L/\omega_p \simeq -0.06608$ , which is consistent with linear Landau theory up to a time  $\omega_p t < 30$ . Then Landau damping is arrested at  $\omega_p t_1 \simeq 50$  and the amplitude of the perturbed mode grows until its saturation at a time  $\omega_p t_2 \simeq 125$ . After  $t > t_2$  and until the end of the simulation, the electrostatic potential oscillates irregularly around a finite amplitude  $e\phi^*/k_B T \simeq 0.01$ , suggesting that the plasma has achieved a time-asymptotic state [2,6].

Trapping of electrons is observed several time-steps after saturation  $t_{\text{trap}} > t_2$ . Indeed, Figs. 1(b)–1(e) show the formation of a vortex centered at  $v = v_L$  that closes completely at  $\omega_p t_{\text{trap}} = 150$ . Due to the symmetry of the distribution function, another vortex is also formed at  $v = -v_L$ . These structures (hereafter referred to as Langmuir vortices) correspond to highly localized deficits or holes in the electron phase-space density that rotate due to resonant interaction with the self-consistent electric potential [5].

Inside the vortex, inward spiral arms are formed due to the nearly parabolic electrostatic potential at the center of the trapping region. This sets a nearly constant bouncing frequency for the trapped electrons [51–54], where electrons closer to the center tend to exhibit coherent motion. Combined with the motion of particles with different velocities, this creates a region of bunched electrons that introduces short-wavelength fluctuations in the electrostatic potential. Toward the borders of the trapping region, the bouncing frequency for electrons varies depending on their location and the motion is less coherent [53]. These structures represent strongly trapped electrons undergoing Langmuir wave resonance.

The observed dynamics in Figs. 1(b)–1(g) is also consistent with the development of the bunching instability shown by Hara *et al.* [52]. Once the instability has saturated, filamentation spreads particles within the hole. The process replicates itself several times during the simulation and becomes quasistationary from  $\omega_p t \simeq 1300$ . Figures 1(f)–1(g) show that the Langmuir vortices and the spiraling arms are persistent until the end of the simulation.

Similar structures have been observed in electron beam-plasma configurations exhibiting instability, in electron beams interacting with a trapping wave [55–58], and in the context of particle trapping generated by an external chirp-drive as

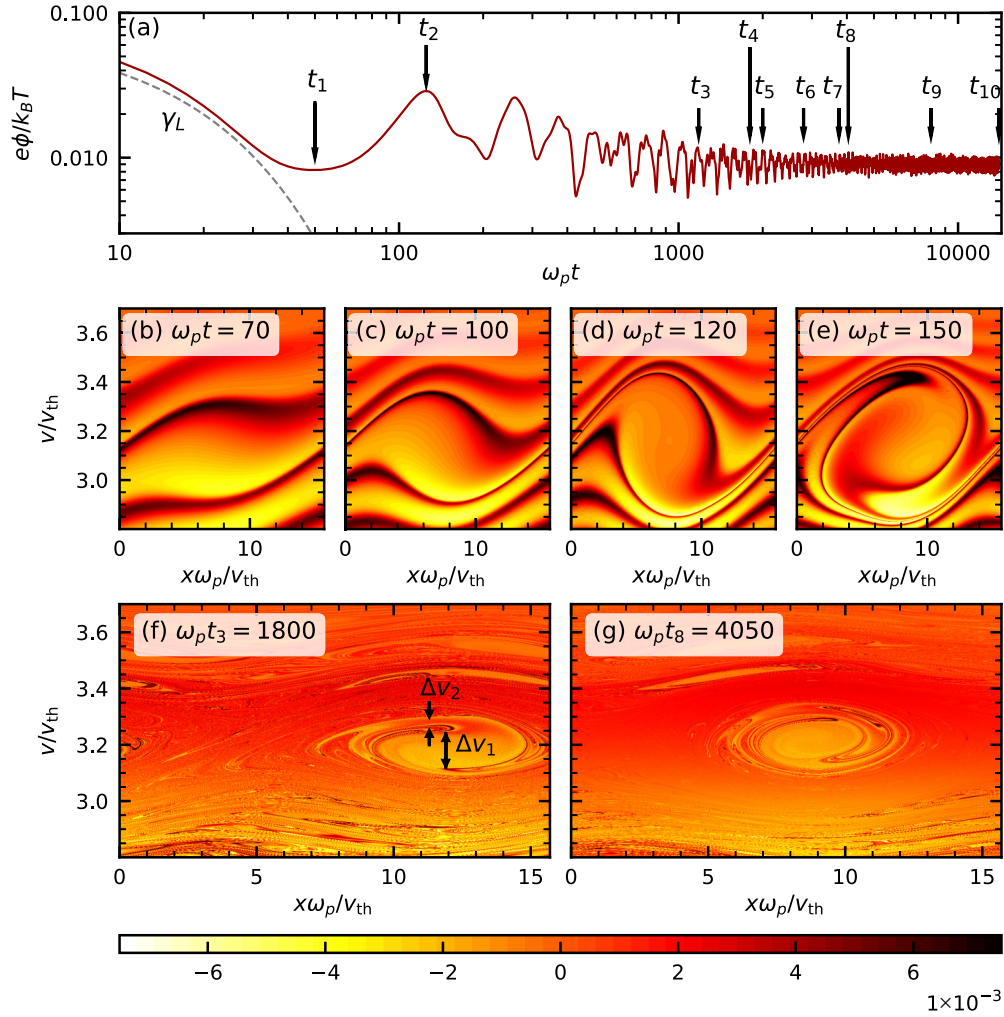


FIG. 1. (a) Log-log time evolution of the envelope of the first Fourier mode of the electrostatic potential. The dashed gray line corresponds to the linear Landau damping prediction. Several times of interest are marked. [(b)–(e)] Electron phase-space snapshots during the formation of the Langmuir electron-hole near  $v = v_L$  at times around  $t = t_2$  and [(f)–(g)] during the quasistationary state  $t \geq t_3$ . The color bar represents the fluctuations  $\delta f$  (in units of  $n_0/v_{th}$ ) of the distribution function with respect to the unperturbed Maxwellian  $f_0$ .

*shark*-like structures within the regions of trapping [4,21]. Studies on the trajectories of beam electrons in a trapping potential show that particles may be classified into a *sea* of particles with chaotic trajectories uniformly distributed and groups of bunched electrons oscillating coherently [57,59,60] with stable trajectories around the structures [61].

#### IV. FORMATION OF SMALL-SCALE PHASE-SPACE VORTICES

Figure 2(a) shows the electrostatic potential  $\phi = \phi(x, t)$  filtered to low frequencies  $|\omega/\omega_p| < 0.6$ . The superposition of counterpropagating Langmuir waves of the same amplitude and phase-speed results in a standing wave with localized positive potential at  $x = L/2$  with enhanced amplitude after  $\omega_p t > 1000$  that seems to be persistent until the end of the simulation. Then, after  $\omega_p t_3 = 1180$  two pairs of solitary and localized electrostatic waves start to propagate with velocities  $|v_1/v_{th}| \simeq 0.06$  and  $|v_2/v_{th}| \simeq 0.014$ . After  $t > t_5$ , various

modes start to grow, propagating with different but constant phase speeds.

Figure 2(b) shows that at  $t = t_3$  a completely closed vortex centered at  $x = L/2$  and  $v = 0$  has formed, as expected from the symmetry in the velocity space and the beating of the waves propagating in the opposite directions. Then disturbances in the filamentary structure of the velocity distribution around  $\pm v_1$  and  $\pm v_2$  evolve into completely closed vortices at  $\omega_p t_4 = 1800$ , as shown in Fig. 2(c). The position-averaged distribution function  $\delta f = \langle f \rangle_x - f_0$ , is shown as white lines in Figs. 2(b)–2(g). In particular, at  $t = t_4$  this quantity exhibits deviations from the regular oscillations seen at  $t = t_3$  specially at  $v = 0, v_1$ , and  $v_2$ . This is a signal that trapping is occurring there, and that these vortices may also be characterized as BGK-like structures [20,59,62].

Note that the velocities of the vortices in Fig. 2(c) are approximately equal to  $|v_1| \simeq \Delta v_1/2$  and  $|v_2| \simeq \Delta v_2/2$ , where  $\Delta v_1/v_{th} \simeq 0.12$  and  $\Delta v_2/v_{th} \simeq 0.03$  are the velocity gaps between the spiral arms rotating inside the Langmuir vortices shown in Fig. 1(f). Although not shown here, as far as we have

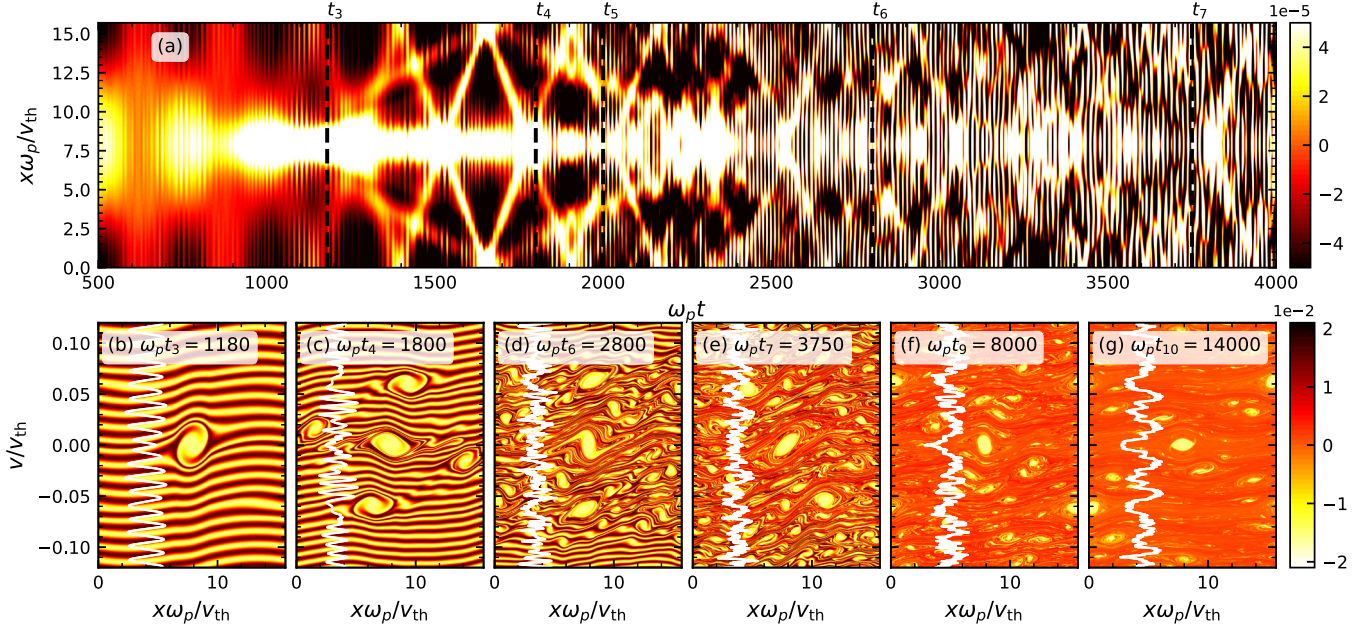


FIG. 2. (a) Electrostatic potential  $\phi = \phi(x, t)$  filtered to low frequencies  $|\omega/\omega_p| < 0.6$ . [(b)–(g)] Fluctuations  $\delta f = f - f_0$ , in units of  $n_0/v_{th}$ , of the electron phase-space distribution for velocities around  $v = 0$  and for  $0 < x < L$ . Solid white lines are the spatially averaged fluctuations of the distribution function  $\delta f(v) = \int dx \delta f(x, v)$ .

checked, this pattern also occurs for different values of the perturbation amplitude  $\varepsilon$ . This suggests that the vortices with velocities  $v_1$  and  $v_2$  result from nonlinear coupling between the spiral arms inside the Langmuir holes.

At times between  $\omega_p t_6 = 2800$  and  $\omega_p t_7 = 3750$ , Figs. 2(d)–2(e) show that vortices of different scale sizes start to fill the electron phase space. This resembles the description for phase-space turbulence in electrostatic plasmas [63–66]. At longer times  $t > t_7$ , Figs. 2(f)–2(g) shows that some of the vortices have disappeared, possibly by coalescence with other holes. The hole at  $v = 0$  is still present at the end of the simulation run, while the holes at  $v_1$  and  $v_2$  look indistinguishable from the remaining holes.

## V. ELECTRON DENSITY $\omega$ - $k$ SPECTRUM

Figure 3 (left) shows snapshots of the full phase-space electron density at several times up to  $\omega_p t = 3750$ . In addition to the vortices discussed before in Figs. 1 and 2, another pair of counterpropagating holes are visible at  $v = \pm 1.07v_{th} \simeq \pm v_L/3$ , and  $v = \pm 1.61v_{th} \simeq \pm v_L/2$ , as shown in Fig. 3(e) at  $\omega_p t_5 = 2000$ . At the times between  $t_5$  and  $t_6$ , vortices of different sizes and localized perturbations in the distribution function appear at several specific velocities within the range  $0.2 \leq |v/v_{th}| \leq 2.1$ , some of them satisfying  $|v| \simeq v_L/n$  with  $2 \leq n \leq 9$ . Then, at times  $\omega_p t > 2800$ , Figs. 2(g) and 2(i) show that localized perturbations eventually evolve to form small-scale holes at velocities greater than the thermal speed, eventually filling the whole phase space. Although not shown here, most of these vortices are eventually dissipated by coalescence or numerical dissipation. However, we still observe the presence of small-scale vortices scattered in phase space at the end of the simulation run at  $\omega_p t = 14000$ , just as described for Fig. 2(g).

Figure 3 (right) shows snapshots of the electron density  $\omega$ - $k$  spectrum at the same times as in Fig. 3 (left). The Fourier spectrum in time is calculated with moving windows so that  $t_i - 600/\omega_p < t < t_i$ . At  $t = t_3$ , a signal with frequency  $\omega = 0$  and spectrum between  $0 < v_{th}k/\omega_p < 4$  can be seen in Fig. 3(b), which is consistent with the formation of a standing wave, and the formation of a stationary hole in phase space as described before. Then Fig. 3(d) shows that two branches of EPWs are excited at a time  $t = t_4$ . Their phase speeds  $|v/v_{th}| \simeq 0.015$  and  $|v/v_{th}| \simeq 0.06$  are approximately equal to the velocities  $v_1$  and  $v_2$  of the four phase-space vortices appearing around  $v = 0$  in Fig. 2(b).

At  $t = t_5$ , Fig. 3(f) shows the excitation of EPW modes of phase speeds  $|v/v_{th}| \simeq 1.07 \simeq v_L/3$  and  $|v/v_{th}| \simeq 1.59 \simeq v_L/2$ , which is consistent with the holes shown in Fig. 3(e). At longer times, Fig. 3(h) shows that the density spectrum is populated by several discrete EPW branches with phase speeds starting from  $v/v_{th} \simeq 1$  towards  $v = 0$ . This is correlated with the velocity of several of the holes in phase space with velocities  $1.2 \leq |v/v_{th}| \leq 1.2$  and other structures with velocities  $1.2 \leq |v/v_{th}| \leq 2.8$  shown in Fig. 3(g). At  $t = t_7$ , the density spectrum in Fig. 3(j) is populated by a large number of EPW branches, resembling the spectrum of spontaneous thermal fluctuations of electrostatic waves [67].

## VI. QUASISTATIONARY STATE

Figure 4(a) shows snapshots of the electric field energy spectrum at three different times, all of them exhibiting a power-law wave-number spectrum  $|E_k|^2 \propto k^\alpha$ . Figure 4(b) shows the evolution of the  $\alpha$  index. This index varies between  $-6 < \alpha < -3$  when the phase space is being filled by small-scale electron holes at times  $400 \lesssim \omega_p t \lesssim 3000$ . In particular, when the central holes are being formed, a peak

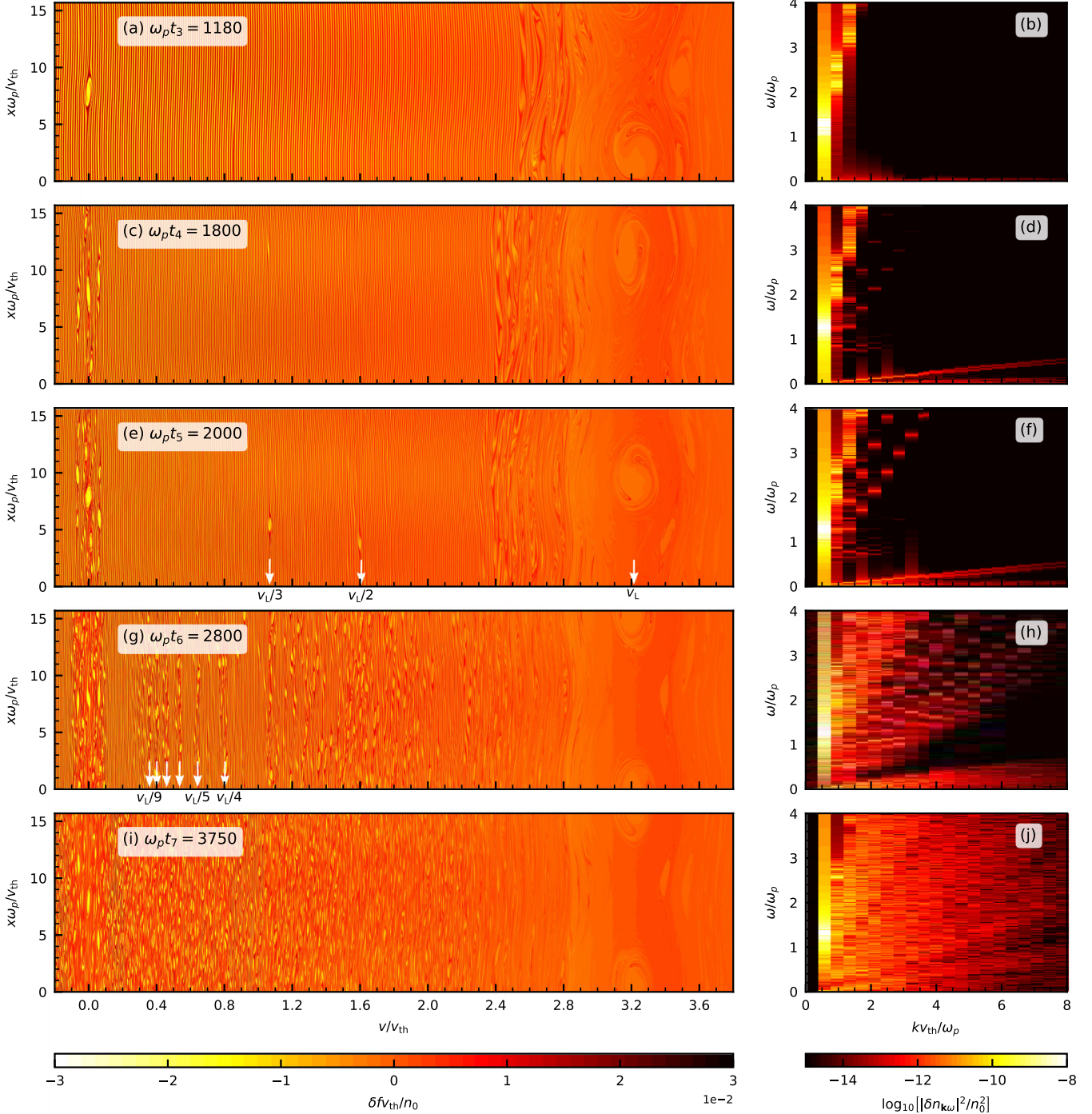


FIG. 3. (Left) Electron phase-space fluctuations  $\delta f = f - f_0$ , normalized to  $n_0/v_{th}$  and (right)  $\omega$ - $k$  spectrum of the normalized electron density  $\delta n_{k\omega}/n_0$  calculated in time windows defined by  $t_i - 600/\omega_p < t < t_i$ , at the times  $t_3$  through  $t_7$  indicated in Fig. 1. The arrows in panels (e) and (g) represent the velocities  $v_L/n$  where some of the vortices are formed, with  $n = \{1, \dots, 9\}$ .

$\alpha_{\text{peak}} \simeq -4$  is found around  $\omega_p t \sim 1200$ . Then  $\alpha$  decreases when further structures are developed in the range  $|v| \leq v_L$ . At  $\omega_p t \sim 4000$ ,  $\alpha$  sets into a quasistationary state reaching the average value  $\alpha_{\text{asympt}} = -4.8074$ . In this state, the phase space is mostly filled with small-scale electron holes. The development of this power-law spectrum suggests that the electric field fluctuations exhibits self-similarity, meaning that the fluctuations at different scales differ only by a scaling factor. This process involves nonlinear interactions between

the nearest modes of the electric field. Although not shown here, the electric field autocorrelation also shows a power-law wave-number spectrum, suggesting that there is an energy cascade process. Due to Gauss's law, the charge density also exhibits a power-law spectrum, so the spatial electron density fluctuations also exhibit self-similarity.

Figure 5 shows snapshots of the velocity spectrum of the space-averaged phase-space distribution fluctuations  $\delta f = \langle f \rangle_x - f_0$ . A sharp peak at  $v = v_0$ , which corresponds to the

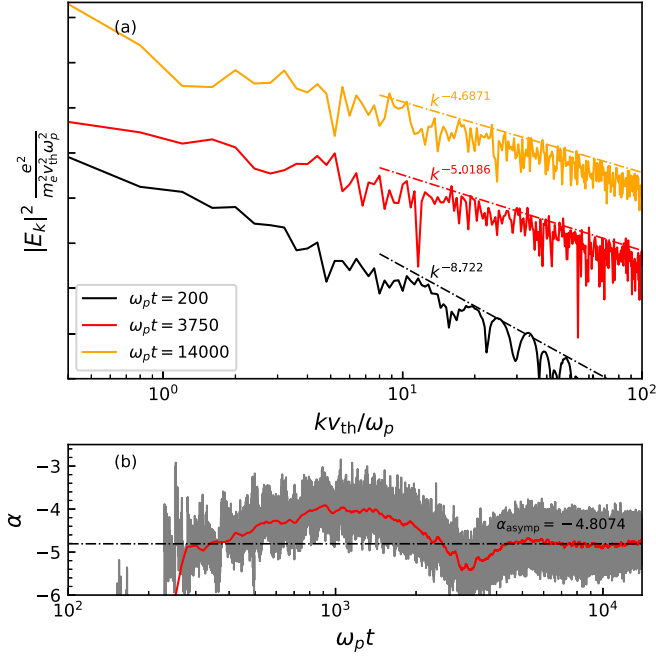


FIG. 4. (a) Snapshots of the electric field energy spectrum at  $\omega_p t = 200, 3750,$  and  $14000$ . Curves are displaced vertically for illustrative purposes. These spectra follow a power law of the form  $|E_k|^2 \propto k^\alpha$ . (b) Time evolution of the index  $\alpha$ . The gray line is the instantaneous value of  $\alpha$ , and the red line is its smoothed pattern.

velocity scale of the filamentation in the distribution function, can be seen in Figs. 5(a)–5(c). Since  $v_0$  increases as time passes, filamentation evolves towards smaller scales in velocity space. In addition, the amplitude of the peak in  $v_0$  decreases with time, which means that filamentation is being dissipated.

After  $\omega_p t = 3750$ , Figs. 5(d)–5(f) show that the spectrum peak amplitude is reduced and becomes comparable to other fluctuations, meaning that filamentation is indistinguishable from other fluctuations in the phase-space distribution function. Then a piecewise power-law spectrum of  $|\delta f_v|^2$  is formed, exhibiting a break-point at  $v = v_0$  which separates a nearly flat spectrum  $|\delta f_v|^2 \propto v^{-\alpha}$  with  $\alpha \approx 0$  for  $v < v_0$ , and a steeper spectrum  $|\delta f_v|^2 \propto v^{-\beta}$  with  $\beta > \alpha$  at smaller scales  $v > v_0$ . At this stage, the distribution function becomes filled with small-scale electron holes, suggesting that the power contained by the filamentation is transferred to the development of small-scale electron holes.

This finding complements the physical picture usually provided for filamentation, where the process is described to continue to unbounded small scales [68–72]. That is, the filamentation evolves toward small scales, but it is self-consistently reduced by the development of small-scale vortices across the distribution. Possibly, small-scale holes could not have been developed if fluctuations were not transported via filamentation. Thus, integration schemes using aggressive velocity filters [68,69,72] hide part of the physics shown in this paper by eliminating the filamentation process early in the simulations.

Figure 6(a) plots the time evolution of  $v_0$ . Before  $\omega_p t < 3750$ , the velocity scale of the filamentation  $v_0$  grows in time with a nearly constant rate  $v_0 \approx 0.4\omega_p t/v_{th}$ . Then

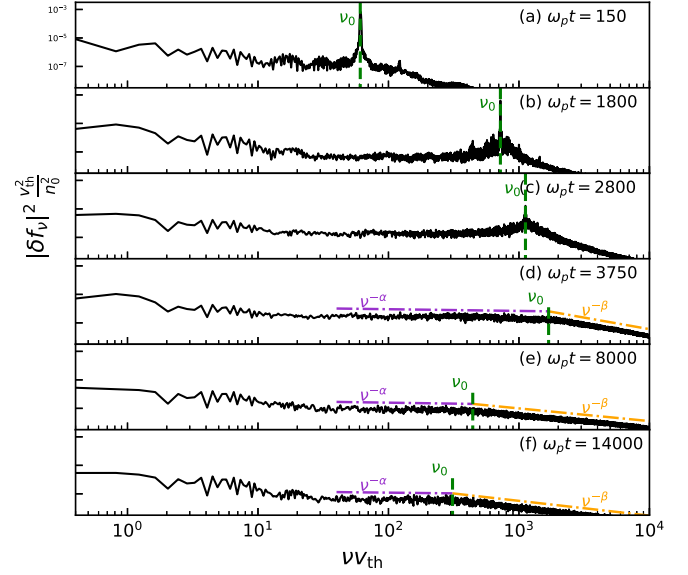


FIG. 5. Fourier transform of the space-averaged distribution function versus the conjugate of the velocity,  $v$ . Snapshots at six different times are shown. In panels (a)–(c), filamentation is clearly observed as a peak in the  $|\delta f_v|^2$  spectrum at  $v = v_0$ . After  $\omega_p t \geq 3750$  [(d)–(f)], filamentation has smoothed, and  $|\delta f_v|^2$  exhibits a break-point at  $v = v_0$  separating a nearly flat spectrum  $|\delta f_v|^2 \propto v^{-\alpha}$  with  $\alpha \approx 0$  for  $v < v_0$ , and a steeper spectrum  $|\delta f_v|^2 \propto v^{-\beta}$  with  $\beta > \alpha$  for  $v > v_0$ .

filamentation becomes indistinguishable from other fluctuations at  $\omega_p t = 3750$ . At this point,  $v_0$  can be identified as the break point in the velocity spectrum of  $|\delta f_v|^2$ . It can be seen that  $v_0$  decreases monotonously and asymptotically approaching to  $v_0 v_{th} \simeq 300$  for  $\omega_p t > 3750$ . Figure 6(b) shows the evolution power-law indices  $\alpha$  and  $\beta$  of the velocity spectrum  $|\delta f_v|^2 \propto v^{-\alpha}$  for  $v < v_0$ , and  $|\delta f_v|^2 \propto v^{-\beta}$  for  $v > v_0$ . At all times,  $\alpha \approx 0$  meaning that a nearly equal amount of kinetic energy per mode is stored at velocity scales  $v < v_0$ . On the other hand,  $\beta$  quickly decreases between  $3750 < \omega_p t < 6000$  and then reaches a quasistationary state around  $\beta \simeq 1$ .

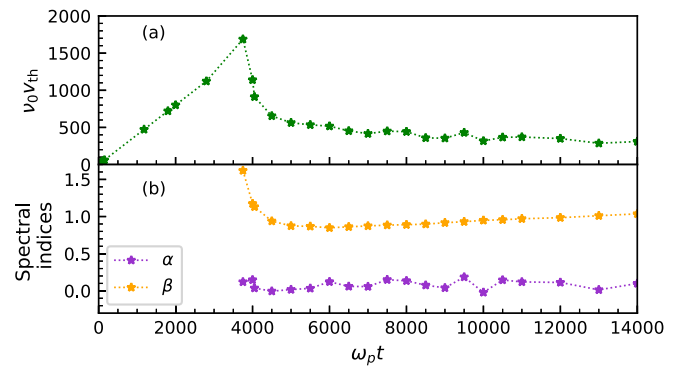


FIG. 6. (a) Time evolution of the velocity scale  $v_0$  shown in Fig. 5. For  $\omega_p t < 3750$ ,  $v_0$  represents the velocity scale of the filamentation in phase space. For  $\omega_p t > 3750$ ,  $v_0$  represents the break-point in  $v$  above which the velocity spectra in  $|\delta f_v|^2$  steepens. (b) Time evolution of the power-law spectral indices of  $|\delta f_v|^2 \propto v^{-\alpha}$  for  $v < v_0$  and  $|\delta f_v|^2 \propto v^{-\beta}$  for  $v > v_0$ .

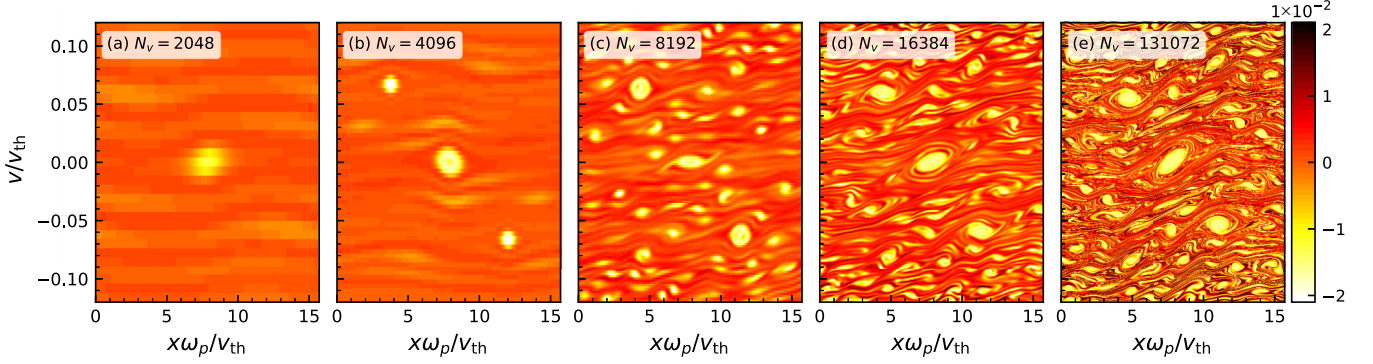


FIG. 7. Electron phase-space snapshots at  $\omega_p t_7 = 3750$  for low velocities near  $v = 0$ . Different numbers of nodes  $N_v$  are used: (a)  $N_v = 2048$ , (b) 4096, (c) 8192, (d) 16 384, and (e) 131 072.

The results from Figs. 3–6 suggest that the phase-space distribution becomes self-similar, i.e., that the small-scale electron holes formed across the distribution follow scaling laws both in the space and velocity domains. As time advances, the large-scale structures in the velocity domain inherit this feature, suggesting that there are nonlinear interaction processes occurring toward structures wider in velocity space. This self-similarity feature is probably of local character, meaning that intermittency is happening in the development of the small-scale electron holes.

## VII. EFFECTS OF THE GRID RESOLUTION

The vortices observed in phase space depend critically on the grid resolution used to numerically resolve the plasma evolution, in particular on the number of nodes  $N_v$  in velocity space. Figure 7 shows snapshots of the phase space near  $v = 0$  at  $\omega_p t = 3750$  for five different simulation runs with different velocity-grid resolutions  $N_v$ . Although the central hole is formed in all cases, Figs. 7(a)–7(c) show that there is a lack of small-scale structures for values of  $N_v < 8192$ , such as the spiraling arms or even the smaller holes formation, compared to cases with higher  $N_v$  values as in Figs. 7(d)–7(e). Simulations with small  $N_v$  cannot resolve fine structures in phase space because the size of the structures reaches the grid size earlier in the simulations. In this situation, some structures do not form or their development is numerically diffusive.

The variations due to changes in the resolution can be quantified with the numerical evolution of invariants of the Vlasov equation. In Fig. 8, we show the time evolution of the invariant  $I_3$  and the entropy  $S$ , defined by

$$I_3 = \int dx dv f^3, \quad (5)$$

$$S = - \int dx dv f \ln f. \quad (6)$$

Although not shown, the relative error of the total energy in all cases is of the order of  $10^{-7}$ , and no significant changes are observed by changing the number of nodes in the physical space,  $N_x$ . Figure 8 shows that a low resolution in velocity space leads to an abrupt increment of the entropy, and an abrupt decrement of the  $I_3$  invariant at earlier stages of the simulation. This is because fluctuations of the distribution function  $f$  reach scales close to the velocity-grid resolu-

tion. Consequently, numerical dissipation is introduced, and structures of the distribution cannot be solved appropriately. Therefore, the presented results corroborate the conclusion of Galeotti and Califano [32], in which the time-asymptotic state is dependent on the dissipation caused by the numerical grid resolution. Even if the value of  $N_v$  is much higher, deviations from invariance in both  $S$  and  $I_3$  are found. In this regard, Fig. 8 suggests that deviations cannot be completely eliminated but at least delayed by increasing the velocity grid resolution  $N_v$ .

## VIII. EFFECTS OF THE PERTURBATION AMPLITUDE

Last, the effects of the perturbation amplitude  $\varepsilon$  on the formation of the first holes around the center of the distribution function are studied. Figure 9 shows the times  $t_c$ , in red, at which the central hole ( $v = 0$ ) is fully formed as in Fig. 2(b) for different values of  $\varepsilon$ . Similarly, the first secondary holes that appear after the central hole as in Fig. 2(c) are also tracked. The corresponding times  $t_s$  are shown with blue error bars in Fig. 9. The holes are considered as fully formed when their spiraling arms with  $\delta f > 0$  coincide for the first time in position space. The error bar size for  $t_c$  and  $t_s$  depends on the sampling ratio of the distribution function around the time of their formation. Simulations consider  $N_v = 8192$  for  $\varepsilon > 0.04$ ,  $N_v = 16\,384$  for  $0.03 < \varepsilon < 0.04$ ,  $N_v = 32\,768$  for  $0.0166 < \varepsilon < 0.03$ ,  $N_v = 65\,536$  for  $0.016 < \varepsilon < 0.0166$ ,

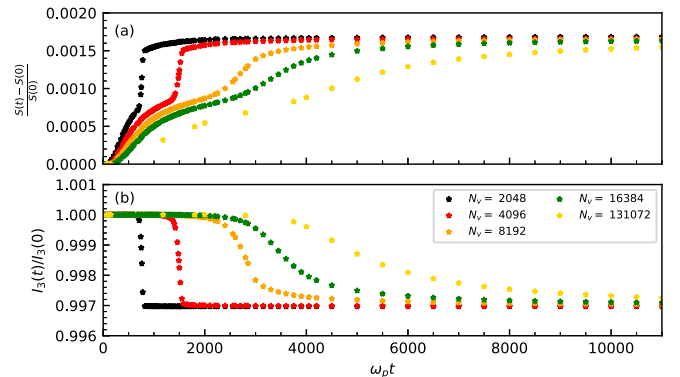


FIG. 8. Time evolution of (a) the entropy and (b) the invariant  $I_3$  of simulations run with different resolution in velocity domain.

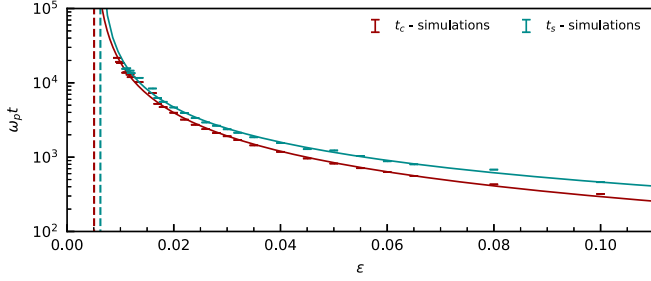


FIG. 9. Times  $t_c$  and  $t_s$  in which the central hole at  $v = 0$  and the secondary holes around it appear, respectively, as a function of the perturbation amplitude  $\varepsilon$ . Solid lines show a power-law fit of the corresponding data. Dashed lines indicate the critical amplitudes for each curve.

$N_v = 131\,072$  for  $0.0135 < \varepsilon < 0.016$ , and  $N_v = 262\,144$  for  $0.0094 < \varepsilon < 0.0135$ . The number of nodes in velocity space is increased because the vortices of interest are formed at longer times for lower values of the perturbation amplitude  $\varepsilon$ . In addition, finer and finer structures develop in velocity space, eventually reaching the grid resolution. Thus,  $N_v$  is increased to avoid early numerical dissipation of these vortices. We checked that different values of  $N_v$  do not alter the time in which the central electron holes start to form. Here all the simulations use  $N_x = 512$ , without significant differences from other values of  $N_x$ .

Figure 9 shows that both times  $t_c$  and  $t_s$  satisfy a power-law dependence on the perturbation amplitude as  $t_i \propto (\varepsilon - \varepsilon_i)^{\mu_i}$ , where  $\varepsilon_i$  represents a critical amplitude above which slow holes with  $v \approx 0$  can appear. For the central vortex, it is found that  $\varepsilon_c = 0.005 \pm 0.002$  and  $\mu_c = -1.4 \pm 0.1$ . For the secondary holes growing from the central hole,  $\varepsilon_s = 0.007 \pm 0.002$  and  $\mu_s = -1.3 \pm 0.1$ . This suggests that the formation of the central and secondary holes in the distribution function may be identified as a second-order transition process [73]. That is, depending on the initial amplitude perturbation  $\varepsilon$ , the phase-space state switches from a phase with pure filamentation to another phase where the filamentation is reduced to form small-scale vortices in phase space.

## IX. CONCLUSIONS

The problem of the time-asymptotic state of a collisionless, initially perturbed Maxwellian distributed electron plasma with immobile ions has been revisited. High-resolution Vlasov-Poisson simulations show the generation of small-scale vortices in phase space other than the already known vortices formed by Landau resonance. Spiraling arms are formed within the Langmuir vortices, corresponding to strongly trapped electrons bouncing within the trapping potential. Then, phase-space vortices are formed near velocities  $v \approx 0$  of the phase-space electron distribution function.

As the plasma evolves, the phase space of electrons is successively filled with small-scale holes below the Langmuir phase speed, with some holes satisfying a simple relationship  $v = v_L/n$ , where  $v_L$  is the Langmuir phase speed, and  $n$  is an integer number. In this process, the energy stored by the filamentation is transferred toward ever smaller scales in

velocity space. This process reduces the filamentation while small-electron holes are formed across the distribution. This indicates that the filamentation has scale bounds in velocity space, rather than continuing indefinitely toward smaller scales [68–72]. The small-scale electron holes seem to persist for long times, and we associate them as small-scale BGK-like states. Accordingly, the physical picture of the time-asymptotic behavior of the perturbed Maxwellian electron plasma is far more complex than the typical description of a state consisting of only two counterpropagating electron holes with velocities near the Langmuir phase speed [1,3,35,36,40,41]. This is more consistent with the notion of multiple small-amplitude BGK-like states [2,39,43].

It is worth noticing that a state consisting of multiple BGK-like structures has already been reported in Maxwellian electron plasmas induced by chirping of an external electrostatic forcing [4]. There the reduction of the frequency displaces the resonance zone toward the center of the distribution function, yielding persisting phase-space holes. However, the state of multiple BGK-like structures reported in this paper is created self-consistently from the initial perturbation of a single mode, without the need for an external forcing [4] nor the presence of an energetic population of particles, such as electron beams [51,52,59,61].

The small-amplitude electron holes are probably grown due to nonlinear wave-wave coupling between spiraling arms inside the Langmuir holes, satisfying a beating condition  $\omega_k = \omega_{k-\ell} + \omega_\ell$ . Then a wave coupling cascade between electron plasma waves (EPWs) starts to fill the  $\omega$ - $k$  power spectrum. Whenever a hole appears, a branch of EPWs with phase speed equal to the velocity of the holes is excited. After the distribution function is filled with small-scale electron holes, the energy spectrum of the electric field and of its autocorrelations are found to obey a power-law dependency on the wave number. This suggests that nonlinear interactions occur between the closest modes so that an energy cascade process is in play.

The velocity spectrum of the space-averaged distribution function exhibits a piecewise power law, with a flat spectrum at large velocity scales, a steepened spectrum for small velocity scales, and a break-point that separates both scales. Thus, fluctuations in the velocity distribution function exhibit self-similarity. As time advances, small-scale electron holes start to localize, suggesting the presence of intermittency, and rendering the self-similarity as local. As the filamentation becomes negligible and small-scale electron holes are formed across the phase space, it is observed that the slope of the electric field energy spectrum acquires a quasisteady behavior.

Also, the time at which the slowest phase-space electron holes are formed follow a power-law function of the initial amplitude perturbation  $\varepsilon$ , suggesting that a process similar to a critical phenomenon is occurring. Thus, there exists a critical amplitude perturbation  $\varepsilon_i$ , below which the phase-space filamentation is reduced indefinitely until it reaches the numerical cell size and above which the filamentation is smoothed to form small-scale electron vortices in phase space.

The findings of this research correspond to an extension of the common interpretation of the time-asymptotic state of nonlinear Landau damping in a one-dimensional setting consisting of only two counterpropagating electron holes. An

interesting question is if this time-asymptotic state could be attained in 2D or 3D simulations. For example, electron holes are observed to propagate stably in multidimensional magnetized plasma simulations [74–76].

This study also highlights the need for high-resolution simulations and algorithms with low numerical dissipation. This is particularly important when addressing time-asymptotic states, because small-scale structures that seem to be relevant in the evolution of the system may not be appropriately resolved. The use of lower resolution, at least in the velocity dependency, leads to an abrupt increment in theoretically invariant quantities (e.g., the entropy and the cubic  $I_3$  invariant) earlier in the simulation. Thus, simulations with low resolution in the velocity space may dissipate the formation of structures in phase space, preventing the plasma from reaching the state observed in our simulations.

The dissipation is intrinsically caused by the numerical scheme chosen to solve the Vlasov-Poisson system. For example, polynomial-splines of second [3] and third order [1,32] have an error of order  $O(N_v^{-n-1})$ , where  $n$  is the order of the interpolation [77–79]. The integration scheme used in this research has spectral interpolation in the velocity dependency, which leads to an error of exponential order decreasing with  $N_v$  [48,49], thus reducing significantly the dissipation by numerical interpolation.

Last, high-order modes must be retained when addressing the velocity dependency in Fourier space. Accordingly, it is advised to consider large integer  $n$  when using velocity filters of the form  $e^{-2n(v/v_{\max})^{2n}}$  [50,80]. This allows the conservation of the  $2n - 1$  moments of the distribution function [68,72,81,82], including the density and flux of particles. Values of  $n$  close to unity introduce strong damping in high-velocity modes, and although they may allow the conservation of the lower moments of the distribution function, they rule out the small-scale vortices observed in this research. In this regard, Cheng and Knorr [80] advised not to use too-large values of  $n$ , because their numerical experiments indicate that the distribution function acquires negative values with increasing  $n$ . However, we used a large resolution in velocity space and the problems found by Cheng and Knorr [80] do not occur.

#### ACKNOWLEDGMENTS

This work has been partially supported by ANID, Chile, through the FONDECYT Grants No. 11180947 and No. 1191351 (R.E.N.) and No. 1161700 (J.A.A.); CONICYT-PAI No. 79170095 (R.E.N.); and National Doctoral Scholarships No. 22182152 and No. 21202472 (H.A.C.), and No. 22182344 and No. 21202616 (J.A.G.).

- 
- [1] G. Manfredi, *Phys. Rev. Lett.* **79**, 2815 (1997).
  - [2] C. Lancellotti and J. J. Dornig, *Phys. Rev. Lett.* **81**, 5137 (1998).
  - [3] M. Raghunathan and R. Ganesh, *Phys. Plasmas* **20**, 032106 (2013).
  - [4] P. Trivedi and R. Ganesh, *Phys. Plasmas* **24**, 032107 (2017).
  - [5] I. Hutchinson, *Phys. Plasmas* **24**, 055601 (2017).
  - [6] A. Ivanov, I. H. Cairns, and P. Robinson, *Phys. Plasmas* **11**, 4649 (2004).
  - [7] C. Lancellotti and J. J. Dornig, *Phys. Rev. E* **68**, 026406 (2003).
  - [8] H. Xu, Z.-M. Sheng, X.-M. Kong, and F.-F. Su, *Phys. Plasmas* **24**, 022101 (2017).
  - [9] Y. Tong, I. Vasko, F. S. Mozer, S. D. Bale, I. Roth, A. V. Artemyev, R. Ergun, B. Giles, P.-A. Lindqvist, C. T. Russell, R. Strangeway, and R. B. Torbert, *Geophys. Res. Lett.* **45**, 11513 (2018).
  - [10] A. Lotekar, I. Vasko, F. Mozer, I. Hutchinson, A. Artemyev, S. Bale, J. W. Bonnell, R. Ergun, B. Giles, Y. V. Khotyaintsev *et al.*, *J. Geophys. Res. Space* **125**, e2020JA028066 (2020).
  - [11] K. Steinvall, Y. V. Khotyaintsev, D. B. Graham, A. Vaivads, P.-A. Lindqvist, C. Russell, and J. Burch, *Geophys. Res. Lett.* **46**, 55 (2019).
  - [12] F. S. Mozer, O. V. Agapitov, B. Giles, and I. Vasko, *Phys. Rev. Lett.* **121**, 135102 (2018).
  - [13] C. Norgren, M. André, A. Vaivads, and Y. V. Khotyaintsev, *Geophys. Res. Lett.* **42**, 1654 (2015).
  - [14] D. B. Graham, Y. V. Khotyaintsev, A. Vaivads, and M. Andre, *J. Geophys. Res. Space* **121**, 3069 (2016).
  - [15] J. Holmes, R. Ergun, D. Newman, N. Ahmadi, L. Andersson, O. Le Contel, R. Torbert, B. Giles, R. Strangeway, and J. Burch, *J. Geophys. Res. Space* **123**, 9963 (2018).
  - [16] J. R. Danielson, F. Anderegg, and C. F. Driscoll, *Phys. Rev. Lett.* **92**, 245003 (2004).
  - [17] R. N. Franklin, S. M. Hamberger, and G. J. Smith, *Phys. Rev. Lett.* **29**, 914 (1972).
  - [18] K. Saeki, P. Michelsen, H. L. Pécseli, and J. J. Rasmussen, *Phys. Rev. Lett.* **42**, 501 (1979).
  - [19] B. Lefebvre, L.-J. Chen, W. Gekelman, P. Kintner, J. Pickett, P. Pribyl, S. Vincena, F. Chiang, and J. Judy, *Phys. Rev. Lett.* **105**, 115001 (2010).
  - [20] C. F. Rupp, R. A. López, and J. A. Araneda, *Phys. Plasmas* **22**, 102306 (2015).
  - [21] P. Trivedi and R. Ganesh, *Phys. Plasmas* **23**, 062112 (2016).
  - [22] F. Valentini, V. Carbone, P. Veltri, and A. Mangeney, *Phys. Rev. E* **71**, 017402 (2005).
  - [23] F. Valentini, *Phys. Plasmas* **12**, 072106 (2005).
  - [24] R. A. López, R. E. Navarro, S. I. Pons, and J. A. Araneda, *Phys. Plasmas* **24**, 102119 (2017).
  - [25] I. B. Bernstein, J. M. Greene, and M. D. Kruskal, *Phys. Rev.* **108**, 546 (1957).
  - [26] H. Schamel, *Phys. Scr.* **20**, 336 (1979).
  - [27] H. Schamel, *Phys. Plasmas* **19**, 020501 (2012).
  - [28] H. Schamel, *Phys. Plasmas* **22**, 042301 (2015).
  - [29] S. Pankavich and R. Allen, *Eur. Phys. J. D* **68**, 363 (2014).
  - [30] G. Manfredi and P. Bertrand, *Phys. Plasmas* **7**, 2425 (2000).
  - [31] R. L. Morse and C. Nielson, *Phys. Rev. Lett.* **23**, 1087 (1969).
  - [32] L. Galeotti and F. Califano, *Phys. Rev. Lett.* **95**, 015002 (2005).
  - [33] F. Califano, L. Galeotti, and A. Mangeney, *Phys. Plasmas* **13**, 082102 (2006).
  - [34] M. Shoucri, *Laser Part. Beams* **35**, 706 (2017).
  - [35] M. Brunetti, F. Califano, and F. Pegoraro, *Phys. Rev. E* **62**, 4109 (2000).
  - [36] S. K. Pandey and R. Ganesh, *Phys. Scr.* **96**, 125616 (2021).

- [37] A. Ghizzo, B. Izrar, P. Bertrand, E. Fijalkow, M. Feix, and M. Shoucri, *Phys. Fluids* **31**, 72 (1988).
- [38] M. Buchanan and J. J. Dorning, *Phys. Rev. Lett.* **70**, 3732 (1993).
- [39] M. Buchanan and J. Dorning, *Phys. Rev. E* **50**, 1465 (1994).
- [40] L. Demeio and P. F. Zweifel, *Phys. Fluids B* **2**, 1252 (1990).
- [41] L. Demeio, *Transp. Theory Stat. Phys.* **30**, 457 (2001).
- [42] E. Fijalkow and L. Nocera, *J. Plasma Phys.* **71**, 401 (2005).
- [43] C. Lancellotti and J. Dorning, *J. Math. Phys.* **40**, 3895 (1999).
- [44] C. Lancellotti and J. Dorning, *Transp. Theory Stat. Phys.* **38**, 1 (2009).
- [45] J. Bezanson, A. Edelman, S. Karpinski, and V. B. Shah, *SIAM Rev.* **59**, 65 (2017).
- [46] E. Sonnendrücker, J. Roche, P. Bertrand, and A. Ghizzo, *J. Comput. Phys.* **149**, 201 (1999).
- [47] R. I. McLachlan and P. Atela, *Nonlinearity* **5**, 541 (1992).
- [48] B. Fornberg and D. M. Sloan, *Acta Numer.* **3**, 203 (1994).
- [49] J. P. Boyd, *Chebyshev and Fourier Spectral Methods* (Springer, Berlin, 2001).
- [50] J. T. Parker and P. J. Dellar, *J. Plasma Phys.* **81**, 305810203 (2015).
- [51] T. M. O’Neil, J. Winfrey, and J. Malmberg, *Phys. Fluids* **14**, 1204 (1971).
- [52] K. Hara, T. Chapman, J. W. Banks, S. Brunner, I. Joseph, R. L. Berger, and I. D. Boyd, *Phys. Plasmas* **22**, 022104 (2015).
- [53] S. Brunner, R. Berger, B. Cohen, L. Hausammann, and E. Valeo, *Phys. Plasmas* **21**, 102104 (2014).
- [54] I. Y. Dodin, P. F. Schmit, J. Rocks, and N. J. Fisch, *Phys. Rev. Lett.* **110**, 215006 (2013).
- [55] T. O’neil and J. Winfrey, *Phys. Fluids* **15**, 1514 (1972).
- [56] A. Bouchoule and M. Weinfeld, *Phys. Rev. Lett.* **36**, 1144 (1976).
- [57] M.-C. Firpo, F. Doveil, Y. Elskens, P. Bertrand, M. Poleni, and D. Guyomarc’h, *Phys. Rev. E* **64**, 026407 (2001).
- [58] N. Carlevaro, M. V. Falessi, G. Montani, and F. Zonca, *J. Plasma Phys.* **81**, 495810515 (2015).
- [59] J. Tennyson, J. Meiss, and P. Morrison, *Physica D* **71**, 1 (1994).
- [60] D. Farina and R. Pozzoli, *Phys. Rev. E* **70**, 036407 (2004).
- [61] J. Adam, G. Laval, and I. Mendonca, *Phys. Fluids* **24**, 260 (1981).
- [62] Y. Hou, M. Chen, M. Yu, B. Wu, and Y. Wu, *Phys. Plasmas* **22**, 122101 (2015).
- [63] T. H. Dupree, *Phys. Fluids* **25**, 277 (1982).
- [64] T. H. Dupree, *Phys. Fluids* **26**, 2460 (1983).
- [65] R. H. Berman, D. J. Tetreault, and T. H. Dupree, *Phys. Fluids* **28**, 155 (1985).
- [66] H. Schamel, D. Mandal, and D. Sharma, *Phys. Plasmas* **24**, 032109 (2017).
- [67] P. H. Yoon, *Phys. Plasmas* **14**, 064504 (2007).
- [68] A. J. Klimas and A. F. Viñas, *J. Plasma Phys.* **84**, 905840405 (2018).
- [69] A. F. Viñas and A. J. Klimas, *J. Comput. Phys.* **375**, 983 (2018).
- [70] N. Besse and E. Sonnendrücker, *J. Comput. Phys.* **191**, 341 (2003).
- [71] L. Einkemmer and C. Lubich, *SIAM J. Sci. Comput.* **40**, B1330 (2018).
- [72] A. J. Klimas and W. M. Farrell, *J. Comput. Phys.* **110**, 150 (1994).
- [73] H. E. Stanley and G. Ahlers, *Introduction to Phase Transitions and Critical Phenomena* (Oxford University Press, New York, 1973).
- [74] M. Wu, Q. Lu, C. Huang, and S. Wang, *J. Geophys. Res. Space* **115**, A10245 (2010).
- [75] I. H. Hutchinson, *J. Plasma Phys.* **84**, 905840411 (2018).
- [76] I. H. Hutchinson, *Phys. Rev. E* **99**, 053209 (2019).
- [77] A. Mangeney, F. Califano, C. Cavazzoni, and P. Travnicek, *J. Comput. Phys.* **179**, 495 (2002).
- [78] P. Colella and P. R. Woodward, *J. Comput. Phys.* **54**, 174 (1984).
- [79] T. Arber and R. Vann, *J. Comput. Phys.* **180**, 339 (2002).
- [80] C. Z. Cheng and G. Knorr, *J. Comput. Phys.* **22**, 330 (1976).
- [81] A. J. Klimas, *J. Comput. Phys.* **68**, 202 (1987).
- [82] A. J. Klimas, A. F. Viñas, and J. A. Araneda, *J. Plasma Phys.* **83**, 905830405 (2017).